

RXTE and *BeppoSAX* Observations of the Transient X-ray Pulsar XTE J1859+083

R. H. D. Corbet^{1,2}, J. J. M. in 't Zand³, A. M Levine⁴, F. E. Marshall⁵

ABSTRACT

We present observations of the 9.8 s X-ray pulsar XTE J1859+083 made with the ASM and PCA on board *RXTE*, and the WFC on board *BeppoSAX*. The ASM data cover a 12 year time interval and show that an extended outburst occurred between approximately MJD 50,250 and 50,460 (1996 June 16 to 1997 January 12). The ASM data excluding this outburst interval suggest a possible modulation with a period of 60.65 ± 0.08 days. Eighteen sets of PCA observations were obtained over an approximately one month interval in 1999. The flux variability measured with the PCA appears consistent with the possible period found with the ASM. The PCA measurements of the pulse period showed it to decrease non-monotonically and then to increase significantly. Doppler shifts due to orbital motion rather than accretion torques appear to be better able to explain the pulse period changes. Observations with the WFC during the extended outburst give a position which is consistent with a previously determined PCA error box, but which has a significantly smaller error. The transient nature of XTE J1859+083 and the length of its pulse period are consistent with it being a Be/neutron star binary. The possible 60.65 day orbital period would be of the expected length for a Be star system with a 9.8 s pulse period.

Subject headings: stars: individual (XTE J1859+083) — stars: neutron — X-rays: binaries

¹University of Maryland, Baltimore County; corbet@umbc.edu

²CRESST/Mail Code 662, NASA Goddard Space Flight Center, Greenbelt, MD 20771

³SRON Netherlands Institute for Space Research, Sorbonnelaan 2, 3584 CA Utrecht, The Netherlands jeanz@sron.nl; Astronomical Institute, Utrecht University, PO Box 80000, 3508 TA Utrecht, The Netherlands

⁴Kavli Institute for Astrophysics and Space Research, MIT, Cambridge, MA 02139

⁵Mail Code 660.1, NASA Goddard Space Flight Center, Greenbelt, MD 20771

1. Introduction

The X-ray source XTE J1859+083 was discovered by Marshall et al. (1999) in observations made with the *Rossi X-ray Timing Explorer (RXTE)* Proportional Counter Array (PCA) on 1999 August 8 (MJD 51,398) during slews between pointed observations of other targets. Although it was not possible to search for pulsations in the slew observation, Marshall et al. (1999) found pulsations at a period of 9.801 ± 0.002 s in an observation made on 1999 August 16. Cross-scan observations with the PCA reported by Marshall et al. (1999) located the source at R.A. = $18^h59.1^m$, decl. = $+8^\circ 15'$ (equinox 2000.0), with an estimated uncertainty of $2'$ (90% confidence). The transient nature of XTE J1859+083 and its pulsations suggest that it might be a member of the Be/neutron star binary class of objects (e.g., Charles & Coe 2006). Such sources are expected to vary on several timescales. Periodic modulation of the X-ray flux on the orbital period may occur if the orbit of the neutron is eccentric. The system may exhibit extended periods of quiescence with no detectable X-ray flux when the circumstellar envelope around the Be star disappears. Less frequently, periods of exceptional brightness, known as Type II outbursts, may also occur, possibly caused by an exceptional expansion of the Be star envelope.

Since the discovery of this source, the only other observations of XTE J1859+083 that have been reported are by Romano et al. (2007) who observed the PCA position on 2007 November 16 to 17 (MJD 54,420.63 - 54,421.98) with the *Swift* X-ray Telescope. Romano et al. (2007) did not detect the source and reported an upper limit of 5×10^{-14} ergs cm^{-2} s^{-1} in the energy range of 0.3 to 10 keV. The non-detection of the source is consistent with XTE J1859+083 being a Be star source during its quiescent phase.

We present here the results of additional observations with the *RXTE* PCA, an improved position from *BeppoSAX* Wide Field Camera (WFC) observations, and an analysis of the *RXTE* All Sky Monitor (ASM) light curve which reveals a possible orbital period. The results of these observations are all consistent with a Be/neutron star classification.

2. Observations

2.1. *RXTE* PCA

The PCA is described in detail by Jahoda et al. (1996, 2006). This instrument consists of five nearly identical Proportional Counter Units (PCUs) sensitive to X-rays with energies between 2 and 60 keV with a total effective area of 6500 cm^2 . The Crab produces 13,000 counts s^{-1} for the entire PCA across the complete energy band. The PCA spectral resolution

at 6 keV is approximately 18%, and the field of view is 1° FWHM.

After the first serendipitous slew observation, pointed observations were carried out with two sets of observations being made every few days over a period of about 38 days. The log of PCA observations is given in Table 1. We analyzed the *RXTE* PCA observations using standard procedures for background subtraction and light curve and spectrum extraction. In Table 1 we give the fluxes resulting from fitting the spectra obtained from each observation with the typical X-ray pulsar model of an absorbed power-law with a high-energy cutoff (White et al. 1983). This model gave a good fit for all observations and we see no large change in spectral parameters as the flux declines with only possibly a small amount of steepening of the spectral slope at lower fluxes. Although some of the spectral parameters, particularly the absorption, are not well constrained at low flux levels we adopt the same spectral model at all flux levels for consistency. The mean spectral parameters are found to be: photon index = 0.84 ± 0.03 , $N_{\text{H}} = 2.1 \pm 0.2 \times 10^{22} \text{ cm}^{-2}$, $E_{\text{cut}} = 6.41 \pm 0.06 \text{ keV}$, and $E_{\text{fold}} = 13.0 \pm 0.3 \text{ keV}$.

We extracted lightcurves from standard 1 data, which have 0.125 sec time resolution, and no energy selection. We made barycenter timing corrections using *faxbary* and combined observations that were close to each other to obtain improved period measurements if phase connection was possible. We used an epoch folding technique to determine pulse period from the resulting 7 light curves. Errors were obtained by determining the periods at which the χ^2 value was 1 less than the peak value.

The pulse timing results are given in Table 2 and plotted in Fig. 1. The period is found to change during the observations with an initial decreasing trend in which the period changes are not monotonic followed by an apparent period increase revealed by a single period measurement. The flux from XTE J1859+083 is seen to initially decline by a factor of more than 10 followed by a low amplitude rebrightening at \sim MJD 51,432.

2.2. *RXTE* ASM

The *RXTE* ASM (Levine et al. 1996) consists of three similar Scanning Shadow Cameras which perform sets of 90 second pointed observations (“dwells”) so as to cover \sim 80% of the sky every \sim 90 minutes. Light curves are available in three energy bands: 1.5 to 3 keV, 3 to 5 keV, and 5 to 12 keV. Source intensities are quoted as the count rates expected if the source was in the center of the field of view of Scanning Shadow Camera 1 in March 1996. With this convention, the Crab Nebula has an intensity of 75.5 counts s^{-1} over the 1.5 - 12 keV energy range and intensities of 26.8 (1.5 - 3 keV), 23.3 (3 - 5 keV), and 25.4 (5 - 12 keV) counts s^{-1}

in each individual band. Observations of blank field regions away from the Galactic center suggest that background subtraction may produce a systematic uncertainty of about 0.1 counts s^{-1} (Remillard & Levine 1997). The ASM light curves used in our analysis span the period from MJD 50,088 to 54,573 (1996 January 6 to 2008 April 17).

The ASM light curve of XTE J1859+083 is plotted in Fig. 2. For this light curve the dwell data were averaged into 2 week time bins. That light curve was then smoothed using an algorithm which replaces each data point with a fraction of its original value plus fractions of the two immediately neighboring points. The factors used for the relative contributions were 50% of the original value weighted by the inverse square of the error on that value, plus 25% of the neighboring points also weighted by the inverse squares of their respective errors. The light curve shows that an extended outburst occurred between approximately MJD 50,250 to 50,460. The peak flux reached during this interval was approximately 1 ASM counts s^{-1} and we note that during the outburst the flux never appears to decrease to a low level. Excluding this period, the mean flux is much lower at approximately 0.1 counts s^{-1} . If this source is a Be star system, as suggested by Romano et al. (2007), then such a long duration event is likely to be a “Type II” outburst during which periodic modulation is not expected to be present (e.g. Stella et al. 1986).

We computed power spectra of the light curve to search for periodic modulation and in all cases the calculation of power spectra employed the “semi-weighting” scheme discussed in Corbet et al. (2007a, b). The power spectrum of the entire light curve (Fig. 3) is dominated by low frequency noise due to the extended outburst. However, the power spectrum of just the ASM light curve obtained since MJD 50,460, after the end of the outburst, shows a peak near a period of 60.6 days (Fig. 3). The nominal false alarm probability (FAP) of obtaining a peak with this strength or greater in the total frequency range considered is approximately 1%. However, for the FAP to be completely valid the number of independent trials, i.e. the frequency range considered, must be decided before a period is searched for (e.g. Scargle 1982). The nominal significance calculation also does not take into account the difficulty to quantify decision to exclude part of the data and that the peak was first noted while searching through ASM light curves of many sources and not just XTE J1859+083. Therefore, the significance of the peak near 60.6 days is <99% and an exact figure cannot be given. We also calculated power spectra of the light curves in the 3 ASM energy bands. None of these power spectra showed a modulation near 60.6 days that was more significant than for the full energy range. In order to further quantify the possible periodic modulation we fitted a sine wave to the light curve since MJD 50,460. This gave a period of 60.65 ± 0.08 days with epoch of maximum flux occurring at MJD $52,549.1 \pm 1.5$. The fitted full amplitude of the modulation is 0.12 ± 0.02 counts s^{-1} , equivalent to approximately 1.6 mCrab, and the mean count rate is 0.092 ± 0.006 cts/s, equivalent to approximately 1.2 mCrab. The ASM

light curve folded on a period of 60.65 days is shown in Fig. 4.

2.3. *BeppoSAX* WFC

The *BeppoSAX* WFC instrument and its observing program are described by Jager et al. (1997) and Verrecchia et al. (2007) respectively. The WFCs were two identical coded mask instruments operating in the range 1.8 - 28 keV. The FOV was 40° by 40° with a FWHM angular resolution of $5'$. The source location accuracy for bright sources in crowded fields was $0.7'$ at 99% confidence level, and larger for sources detected at lower significance levels. The on-axis sensitivity was between 2 to 10 mCrab for a typical *BeppoSAX* WFC observation of 3×10^4 s, and depended on the intensities of other sources in the same FOV. The WFCs pointed in opposite directions from each other and at 90° from the Narrow Field Instruments also on board *BeppoSAX*. The WFCs operated between 1996 April 30 (MJD 50,203) and 2002 April 30 (MJD 52,394) and covered the entire sky multiple times.

During 1996 to 2002 XTE J1859+083 was in a *BeppoSAX* WFC FOV 115 times for a total estimated net exposure time of 1.5 Msec. We searched for the combination of images that produced the most significant detection of XTE J1859+083. It was found that data taken between MJD 50,340.65 and 50,395.91, i.e. during the period when the ASM light curve indicates that XTE J1859+083 was in an extended outburst, gave the best results, and the signal-to-noise ratio is 16.7 for this interval. The count rate in the WFC was found to be too low to allow useful spectroscopy to be obtained. The best-fit source coordinates are: R.A. = $18^h 59^m 2.4^s$, decl. = $+8^\circ 13' 57''$ (equinox 2000.0) with a 99% confidence error radius of $1.6'$. For a Gaussian error distribution this translates to a $1.0'$ radius at a 90% confidence level. The equivalent Galactic coordinates are $l = 41.12^\circ$, $b = 2.07^\circ$. This WFC error region has a four times smaller area than the previously determined PCA position. Outside this time interval we found no significant detection of XTE J1859+083 in individual observations or combinations of observations. However, the WFC observations containing XTE J1859+083 were very non-uniform and there was more coverage during the earlier part of the SAX mission, when the source was coincidentally experiencing the extended outburst.

We plot both the PCA and WFC error regions on red and blue Digitized Sky Survey images in Fig. 6. The DSS images are reported to be complete down to $V = 21$ (Monet et al. 2003). Several stars are visible in the overlap of the error boxes and the brightest object is USNO-B1.0 0982-0467446 ($B = 14.7$)/2MASS 18590277+0814220 ($I = 11.7$). However, despite the reduction in the size of the error box, without additional information on the objects in the error box we cannot yet determine the optical counterpart.

3. Discussion

A 60.65 day period would be consistent with the orbital period expected for a Be star system containing a 9.8 s X-ray pulsar based on the correlation between orbital and pulse periods for this type of system (Corbet 1986). However, the 60.65 day period is of modest statistical significance in the ASM power spectrum. We therefore investigate whether the PCA pulse timing and flux measurements can help determine whether this is indeed the orbital period of the system.

We first consider whether the changes in the pulse period could be caused by accretion torques or orbital Doppler shifts. Joss & Rappaport (1984) calculate that the spin-up rate can be approximately expressed by: $\dot{P}/P \sim 3 \times 10^{-5} (P/1s) (L_X/10^{37} \text{ erg s}^{-1})^{6/7}$. If the initial period decrease seen in XTE J1859+083 was caused by accretion torques, it thus requires a luminosity of about $10^{39} \text{ ergs s}^{-1}$. However, the brightest flux seen with the PCA only corresponds to about $10^{36} \text{ ergs s}^{-1}$ at 10 kpc. Period change primarily caused by accretion torques thus appears to be unlikely.

The mass function of a binary is given by $f(M) = P_{orb} K^3 (1 - e)^{3/2} / 2\pi G$. This corresponds to the minimum possible mass of the primary star. We can estimate the mass function of XTE J1859+083 for the assumptions that the orbital period is 60.65 days and that the observed pulse period changes are due to orbital motion. Assuming a circular orbit for simplicity, the observed maximum and minimum pulse periods imply a velocity semi-amplitude of $\gtrsim 100 \text{ km s}^{-1}$ which implies a mass function of $\gtrsim 6 M_\odot$. The orbit is not fully sampled which suggests the velocity amplitude should be larger than implied by the limited pulse period measurements, and hence that the mass function would be larger. Conversely, if the orbit is significantly eccentric, as is common for some Be star systems, then the mass function could be smaller. Nevertheless, it appears that it is not unrealistic to account for the observed pulse period changes by orbital Doppler motion. It is thus probable that orbital Doppler shifts were more important than accretion torques in producing the observed pulse period changes. We note, however, that the period changes are not completely smooth. This suggests that accretion torques may be more important than the simple estimate above implies.

We investigated whether it was possible to determine orbital parameters by fitting the pulse period measurements. Since there are only 7 period measurements, and the period increase is only indicated by a single measurement, this severely limits our ability to determine the orbital parameters. Keeping the orbital period fixed at the value measured with the ASM, we fitted a circular orbit. This resulted in an orbit with a very large velocity amplitude with a correspondingly unrealistically large mass function. We conclude that more extensive pulse period measurements are required before a reliable orbital solution can be

determined. In particular, period measurements should ideally span at least one complete 60.65 day cycle.

We next consider whether the PCA flux modulation is consistent with the proposed period. In Fig. 4 we plot the PCA fluxes on the folded ASM flux with the PCA peak flux arbitrarily normalized to facilitate comparison of the shape of the modulation. It is seen that the peak PCA flux and decline from this have similar behavior to the folded ASM flux. However, the last few PCA observations fall below the average ASM flux. In Fig. 5 we overplot the PCA fluxes and the ASM fluxes obtained during the same time. Due to the lower sensitivity of the ASM compared to the PCA a 5 day time resolution was used for the ASM light curve and this was then smoothed using the same algorithm described in Section 2.2. We convert the ASM count rate to flux using the spectrum derived in Section 2.1 which gives a conversion factor of $0.1 \text{ ASM counts s}^{-1} \simeq 3.1 \times 10^{-11} \text{ ergs cm}^{-2} \text{ s}^{-1}$. There is reasonable agreement of the flux level seen in the two instruments with the exception that the flux measured from the slow observations appears brighter than that measured with the ASM. Note, however, that the PCA flux is derived from a very brief observation whereas the ASM light curve uses smoothed 5 day bins. The ASM data suggest that a modest outburst at the time of the next predicted maximum occurred shortly after the PCA observations ceased. It thus appears that the light curve obtained with the PCA is consistent with the proposed 60.65 day modulation. If the primary of the system is a Be star then modulation of the light curve on the orbital period would depend on the structure of the envelope around the Be star, i.e. its density and velocity and the orbit of the neutron star. Variability of the properties of the Be star envelope, as would be expected to occur, would lead to changes in the orbital modulation of the light curve. If the orbital parameters of XTE J1859+083 can be confirmed, and the optical counterpart identified, then it may be possible to derive parameters of the Be envelope from the modulation of the light curve and emission at $\text{H}\alpha$ which would come from the envelope and hence also provide information on the physical conditions of the envelope.

We note that the *Swift* non-detection of XTE J1859+083 (Romano et al. 2007) occurred at a phase of 0.85. The folded ASM light curve (Fig. 4) shows that XTE J1859+083 has generally been bright at that phase, suggesting that the source may have been in an extended inactive state. The occurrence of extended inactive states where the outbursts near periastron passage cease is common for Be/neutron star binaries (e.g. Charles & Coe 2006).

4. Conclusion

The spectral, flux variability, and timing properties of XTE J1859+083 appear to be consistent with a Be star X-ray binary classification. XTE J1859+083 appears to have exhibited the three types of emission state commonly seen in this type of source: (i) a bright Type II outburst with no periodic modulation; (ii) a lower luminosity state during which the PCA observations were made and during which periodic modulation of the flux may have occurred; and (iii) a quiescent state during which no emission was detectable. Additional observations to further reduce the size of the error box would be valuable, and these should preferably be carried out at the peak of the candidate 60.65 day period. If the source enters another extended bright phase then additional pulse timing measurements should be able to fully determine the orbital parameters of this system.

We thank Cees Bassa for making the DSS finding charts.

REFERENCES

- Charles, P.A., & Coe, M.J. 2006, in *Compact Stellar X-ray Sources*, ed. W.H.G. Lewin & M. van der Klis (Cambridge: Cambridge Univ. Press), 215
- Corbet, R.H.D. 1986, *MNRAS*, 220, 1047
- Corbet, R.H.D., Markwardt, C.B., & Tueller, J. 2007a, *ApJ*, 655, 458
- Corbet, R., Markwardt, C., Barbier, L., Barthelmy, S., Cummings, J., Gehrels, N., Krimm, H., Palmer, D., Sakamoto, T., Sato, T., & Tueller, J. 2007b, proceedings of “The Extreme Universe in the Suzaku Era”, Kyoto, Japan, December 4-8, 2006. *Progress of Theoretical Physics Supplement*, 169, 200
- Jager, R., Mels, W. A., Brinkman, A. C., Galama, M. Y., Goulooze, H., Heise, J., Lowes, P., Muller, J. M., Naber, A., Rook, A., Schuurhof, R., Schuurmans, J. J., & Wiersma, G. 1997, *A&AS*, 125, 557
- Jahoda, K., Swank, J. H., Giles, A. B., Stark, M. J., Strohmayer, T., Zhang, W., & Morgan, E. H. 1996 *Proc. SPIE*, 2808, 59
- Jahoda, K., Markwardt, C. B., Radeva, Y., Rots, A. H., Stark, M. J., Swank, J. H., Strohmayer, T. E., Zhang, W. 2006, *ApJS*, 163, 401
- Joss, P.C., & Rappaport, S. 1984, *ARA&A*, 22, 537
- Levine, A.M., Bradt, N., Cui, W., Jernigan, J.G., Morgan, E.H., Remillard, R., Shirey, R.E., & Smith, D.A. 1996, *ApJ*, 469, L33

- Marshall, F. E., in 't Zand, J. J. M., Strohmayer, T., & Markwardt, C. B. 1999, IAUC 7240
- Monet, D.G., et al. 2004, AJ, 125, 984
- Remillard, R.A., & Levine, A.M. 1997, in All-Sky X-ray Observations in the Next Decade, ed. M. Matsuoka & N. Kawai (Wako: RIKEN), 29
- Romano, P., Mangano, L., Sidoli, V., & Mereghetti, S. 2007, ATEL 1287
- Scargle, J.D., 1982, ApJ, 263, 835
- Stella, L., White, N.E., & Rosner, R. 1986, ApJ, 308, 669
- Verrecchia, F., in't Zand, J. J. M., Giommi, P., Santolamazza, P., Granata, S., Schuurmans, J. J., & Antonelli, L. A. 2007, A&A, 472, 705
- White, N.E., Swank, J.J., & Holt, S.S. 1983, ApJ, 270, 711

Table 1. *RXTE* PCA Observations of XTE J1859+083

ID	Start Time	End Time	Length (s)	2 - 10 keV Flux (ergs cm ⁻² s ⁻¹) $\times 10^{-11}$	Photon Index	N_{H} (10 ²² cm ⁻²)	E_{cut} (keV)	E_{fold} (keV)	Count Rate	χ^2_{ν}	Phase Range
1	6.93272	6.98342	1184	16.15 +0.10, -0.09	0.93 \pm 0.21	2.98 \pm 1.58	6.75 \pm 0.36	13.30 \pm 0.88	68.02 \pm 0.45	0.83	0.1695 - 0.1704
2	8.23485	8.33245	4976	15.86 +0.04, -0.05	0.75 \pm 0.11	1.53 \pm 0.76	6.39 \pm 0.20	13.54 \pm 0.52	64.50 \pm 0.23	1.06	0.1910 - 0.1926
3	9.85825	9.87297	1072	14.39 +0.12, -0.11	0.76 \pm 0.31	0.95 \pm 2.32	7.15 \pm 0.50	15.07 \pm 1.37	41.83 \pm 0.39	0.47	0.2178 - 0.2180
4	11.16430	11.18726	1952	14.25 +0.07, -0.06	0.91 \pm 0.19	2.54 \pm 1.42	6.63 \pm 0.30	13.69 \pm 0.77	73.93 \pm 0.41	0.91	0.2393 - 0.2397
5	12.16282	12.18671	1984	13.01 +0.07, -0.06	0.69 \pm 0.16	1.54 \pm 0.99	6.05 \pm 0.30	12.12 \pm 0.78	70.65 \pm 0.40	0.77	0.2558 - 0.2562
6	13.22880	13.25615	2144	12.55 +0.06, -0.07	0.95 \pm 0.22	2.99 \pm 1.52	6.28 \pm 0.36	13.37 \pm 0.96	50.73 \pm 0.33	0.44	0.2734 - 0.2738
7	14.03024	14.04171	976	11.89 +0.11, -0.08	0.75 \pm 0.31	1.72 \pm 2.04	6.30 \pm 0.50	12.26 \pm 1.23	47.43 \pm 0.47	1.21	0.2866 - 0.2868
8	14.09300	14.11300	1568	12.00 +0.09, -0.07	0.99 \pm 0.27	3.85 \pm 1.91	6.29 \pm 0.39	12.11 \pm 0.95	47.73 \pm 0.38	0.80	0.2876 - 0.2879
9	15.09189	15.14485	1584	10.70 +0.12, -0.08	0.97 \pm 0.33	2.09 \pm 2.40	6.61 \pm 0.60	15.92 \pm 1.87	29.44 \pm 0.31	0.83	0.3041 - 0.3049
10	15.17253	15.18319	912	10.90 +0.09, -0.10	0.98 \pm 0.30	3.04 \pm 2.00	6.14 \pm 0.51	13.36 \pm 1.41	71.33 \pm 0.64	0.62	0.3054 - 0.3056
11	17.02948	17.03893	800	9.05 +0.13, -0.15	0.90 \pm 0.47	1.63 \pm 3.68	7.00 \pm 0.74	13.34 \pm 1.89	24.39 \pm 0.42	0.90	0.3360 - 0.3362
12	17.08985	17.11022	1584	9.37 +0.11, -0.11	0.73 \pm 0.35	0.65 \pm 2.42	6.59 \pm 0.57	13.61 \pm 1.54	25.22 \pm 0.30	0.98	0.3370 - 0.3373
13	19.15636	19.17852	1888	7.27 +0.07, -0.08	0.99 \pm 0.31	2.93 \pm 2.10	6.21 \pm 0.48	12.59 \pm 1.30	37.37 \pm 0.38	1.08	0.3711 - 0.3715
14	19.22750	19.25004	1920	7.07 +0.07, -0.07	1.02 \pm 0.33	3.27 \pm 2.35	6.25 \pm 0.46	12.16 \pm 1.19	36.46 \pm 0.37	0.92	0.3723 - 0.3726
15	20.31178	20.32995	752	5.34 +0.14, -0.13	0.95 \pm 0.74	2.43 \pm 4.88	6.27 \pm 0.92	10.73 \pm 2.08	20.27 \pm 0.49	0.72	0.3901 - 0.3904
16	20.38468	20.39592	832	5.20 +0.15, -0.16	1.00 \pm 0.81	0.89 \pm 5.49	6.40 \pm 1.37	14.52 \pm 4.17	13.73 \pm 0.38	0.85	0.3913 - 0.3915
17	25.97901	25.99036	128	1.54 +0.32, -0.39	1.17 \pm 7.20	20.97 \pm 52.43	6.45 \pm 2.48	3.53 \pm 2.58	5.15 \pm 1.23	0.56	0.4836 - 0.4838
18	26.01698	26.02911	1040	1.64 +0.13, -0.12	1.42 \pm 1.99	3.39 \pm 13.01	6.67 \pm 2.64	11.82 \pm 7.15	5.80 \pm 0.42	0.48	0.4842 - 0.4844
19	28.97416	29.02578	1280	2.58 +0.11, -0.11	1.81 \pm 0.95	7.94 \pm 7.20	6.13 \pm 1.03	7.98 \pm 1.89	9.40 \pm 0.38	0.50	0.5330 - 0.5338
20	32.23217	32.24102	768	3.54 +0.15, -0.15	0.97 \pm 0.81	1.34 \pm 4.85	5.76 \pm 2.57	17.94 \pm 10.26	16.20 \pm 0.50	0.53	0.5867 - 0.5868
21	32.30152	32.31536	1056	3.49 +0.13, -0.12	1.15 \pm 0.85	3.23 \pm 6.21	6.73 \pm 2.09	20.41 \pm 8.23	17.16 \pm 0.43	1.12	0.5878 - 0.5881
22	35.87078	35.91116	1008	2.69 +0.12, -0.12	1.00 \pm 1.10	2.52 \pm 6.69	6.14 \pm 1.43	10.49 \pm 3.29	9.37 \pm 0.41	0.90	0.6467 - 0.6473
23	39.01763	39.03967	1808	1.30 +0.09, -0.11	1.22 \pm 1.84	0.37 \pm 11.24	6.44 \pm 1.67	9.31 \pm 3.49	4.51 \pm 0.30	1.01	0.6986 - 0.6989
24	41.74263	41.74866	528	0.51 +0.09, -0.14	0.56 \pm 10.04	0.43 \pm 32.94	6.19 \pm 3.05	3.96 \pm 4.42	2.51 \pm 0.66	0.69	0.7435 - 0.7436
25	41.81208	41.83269	1744	0.52 +0.09, -0.10	1.80 \pm 3.09	5.67 \pm 22.59	6.79 \pm 1.02	1.68 \pm 1.00	0.67 \pm 0.30	0.90	0.7446 - 0.7450
26	44.73542	44.74588	896	0.57 +0.09, -0.12	2.37 \pm 3.94	1.52 \pm 20.96	3.65 \pm 10.32	9.99 \pm 34.44	2.52 \pm 0.43	0.73	0.7928 - 0.7930
27	44.82212	44.83272	816	0.47 +0.09, -0.14	0.89 \pm 3.27	0.00 \pm 52.25	7.31 \pm 1.28	0.73 \pm 1.25	-0.58 \pm 0.43	1.00	0.7943 - 0.7944

Note. — Start and end times are in units of MJD - 51,400. The flux is not corrected for absorption. Flux errors are 1 σ confidence intervals obtained from fitting the spectra with all parameters fixed at the mean values from fitting all spectra, with the exception of the normalization and E_{fold} . The phase range is for a period of 60.65 days and phase zero corresponds to MJD 52,549.1.

Table 2. *RXTE* PCA Pulse Period Measurements of XTE J1859+083

Observation Numbers	Start Time (MJD)	End Time (MJD)	Period (s)
1, 2	51406.93272	51408.33245	9.80098 ± 0.00002
3, 4	51409.85825	51411.18726	9.79773 ± 0.00001
5, 6	51412.16282	51413.25615	9.79819 ± 0.00003
7, 8, 9	51414.03024	51415.14485	9.79717 ± 0.00001
10, 12	51415.17253	51417.11022	9.79526 ± 0.00001
13, 16	51419.15636	51420.39592	9.79532 ± 0.00003
20, 21, 22	51432.23217	51435.91116	9.80170 ± 0.00001

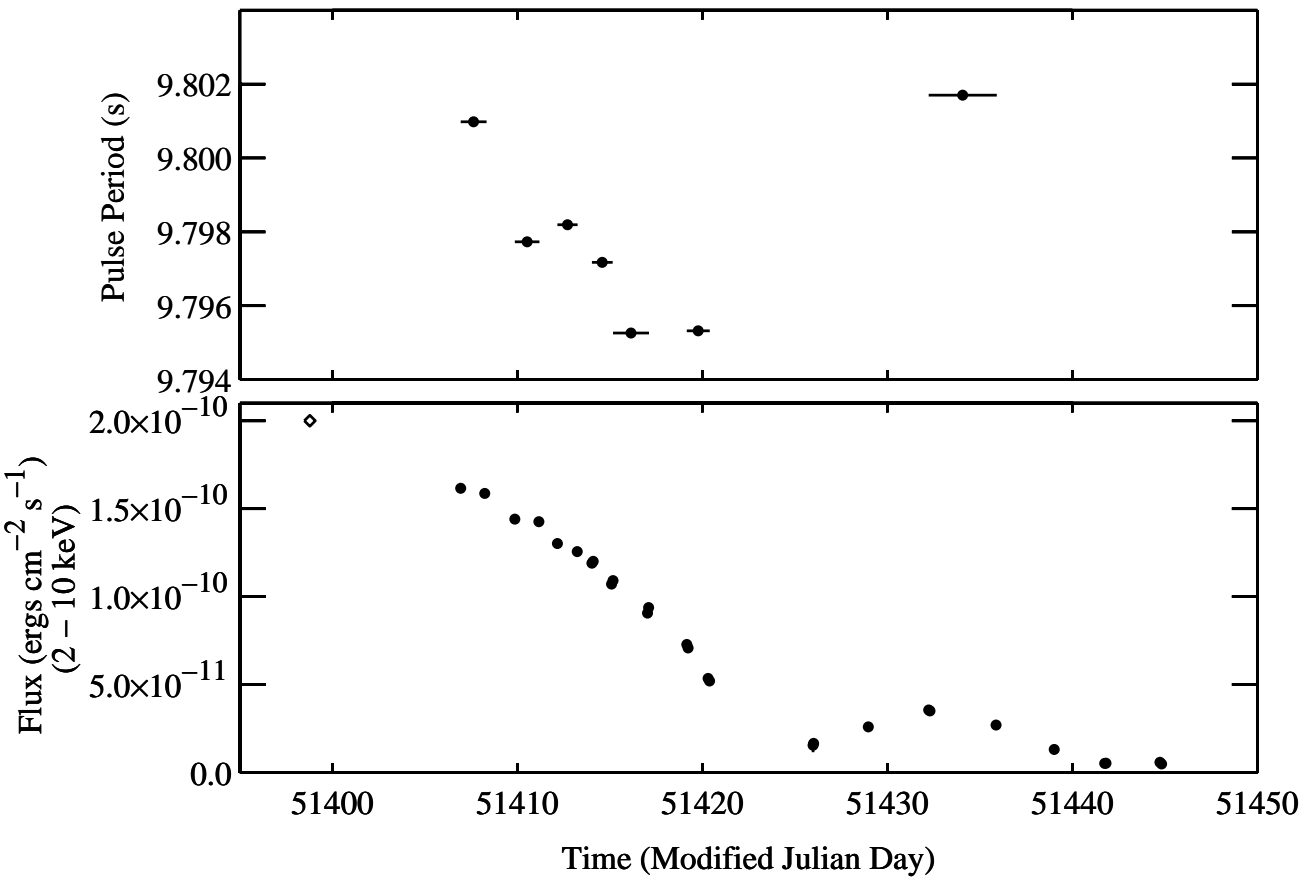


Fig. 1.— *RXTTE* PCA measurements of the flux (lower panel) and pulse period (upper panel) of XTE J1859+083. Pulse period measurements were not possible for observations with low count rates or short durations. Flux and pulse period values are also given in Tables 1 and 2 with the exception of the first flux measurement, marked with a diamond, which is taken from Marshall et al. (1999) and for which no error is available. The errors on the pulse period and flux measurements are smaller than the symbol size.

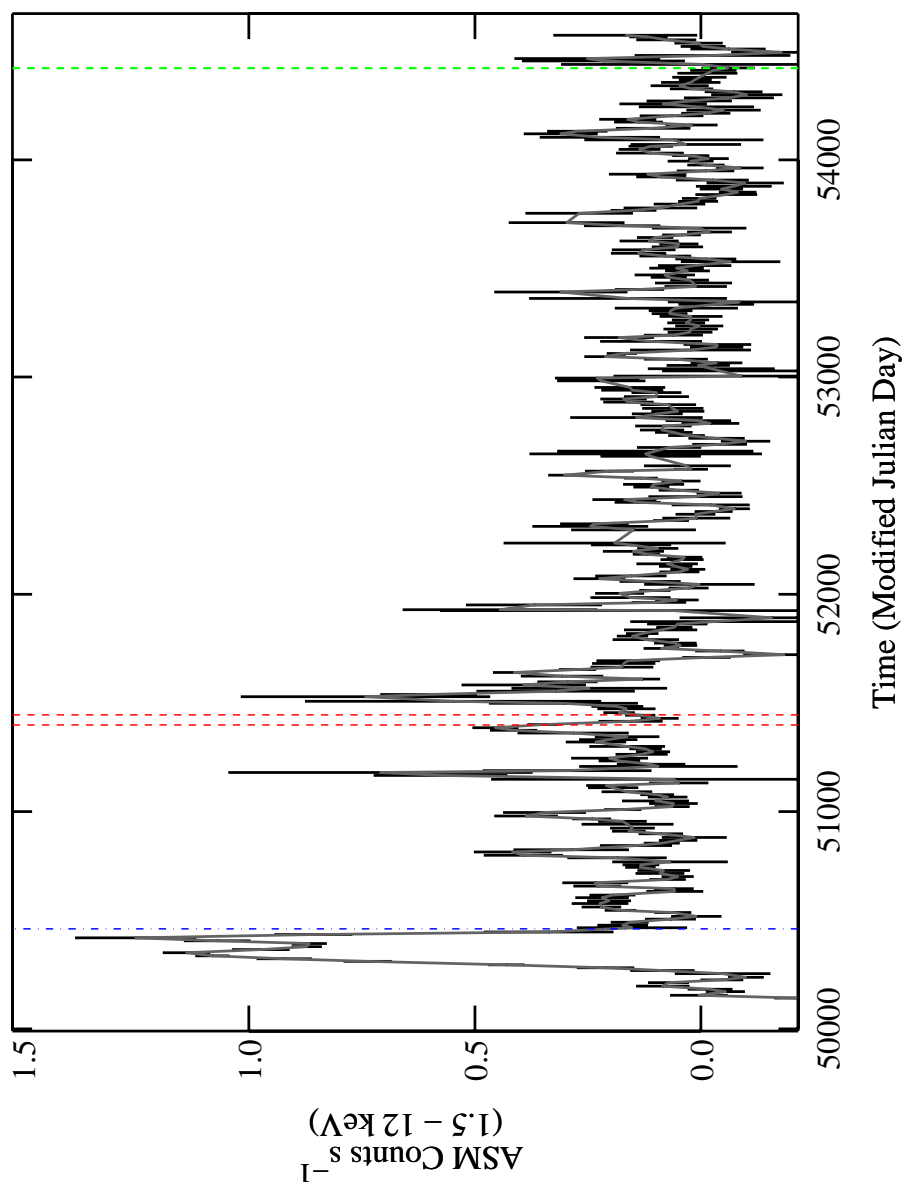


Fig. 2.— The *RXTE* ASM light curve of XTE J1859+083. The light curve has two week time bins which were then smoothed using the algorithm described in Section 2.2. The vertical dot-dashed blue line indicates MJD 50,460, before which the source may have experienced a “Type II” outburst. The red vertical dashed lines at MJD 51,398.78 and 51,444.82 indicate the interval during which the PCA observations were made. The green vertical dashed lines at MJD 54420.63 and 54421.98 indicate the time during which Swift observations failed to detect the source (Romano et al. 2007).

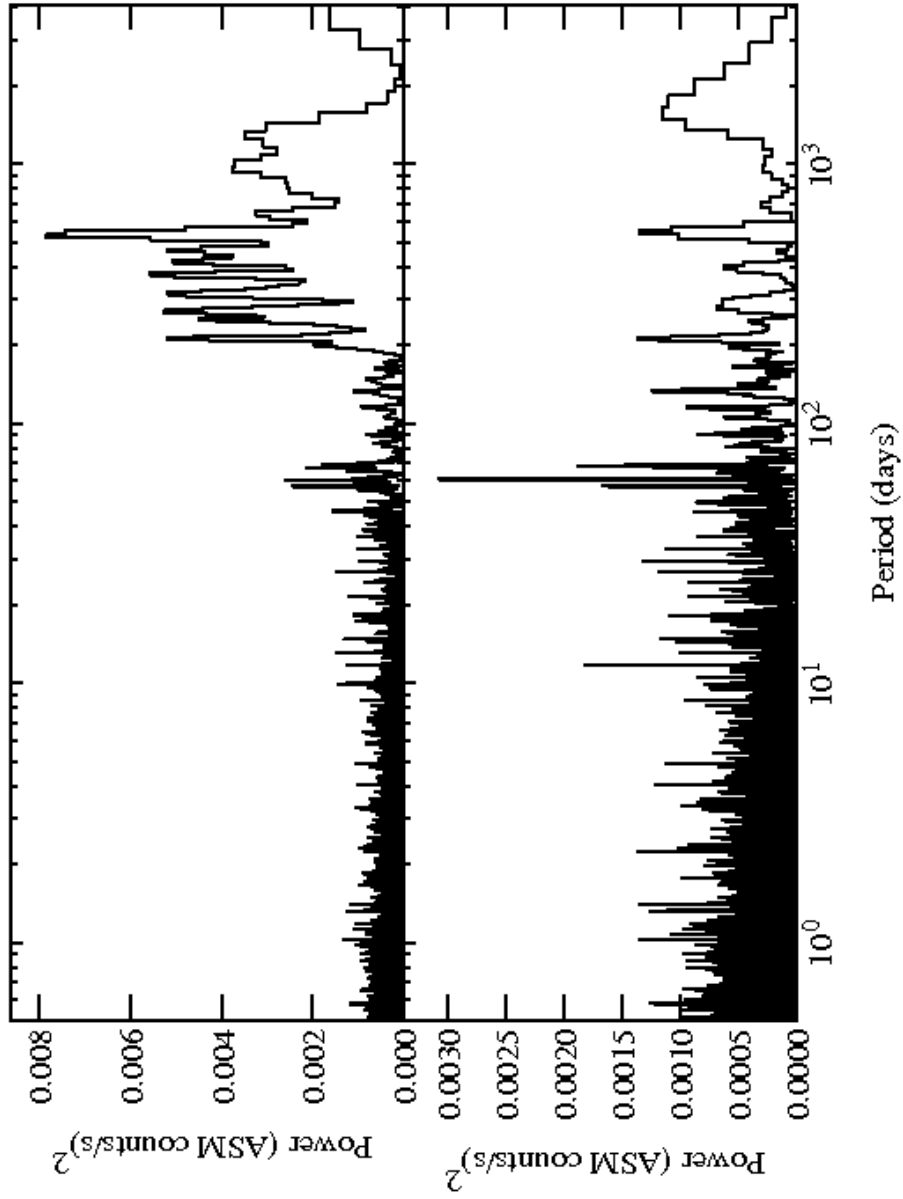


Fig. 3.— Power spectra of the *RXTE* ASM light curve of XTE J1859+083. The upper panel shows the power spectrum of the entire light curve. The lower panel shows the power spectrum using only observations made after MJD 50,460.

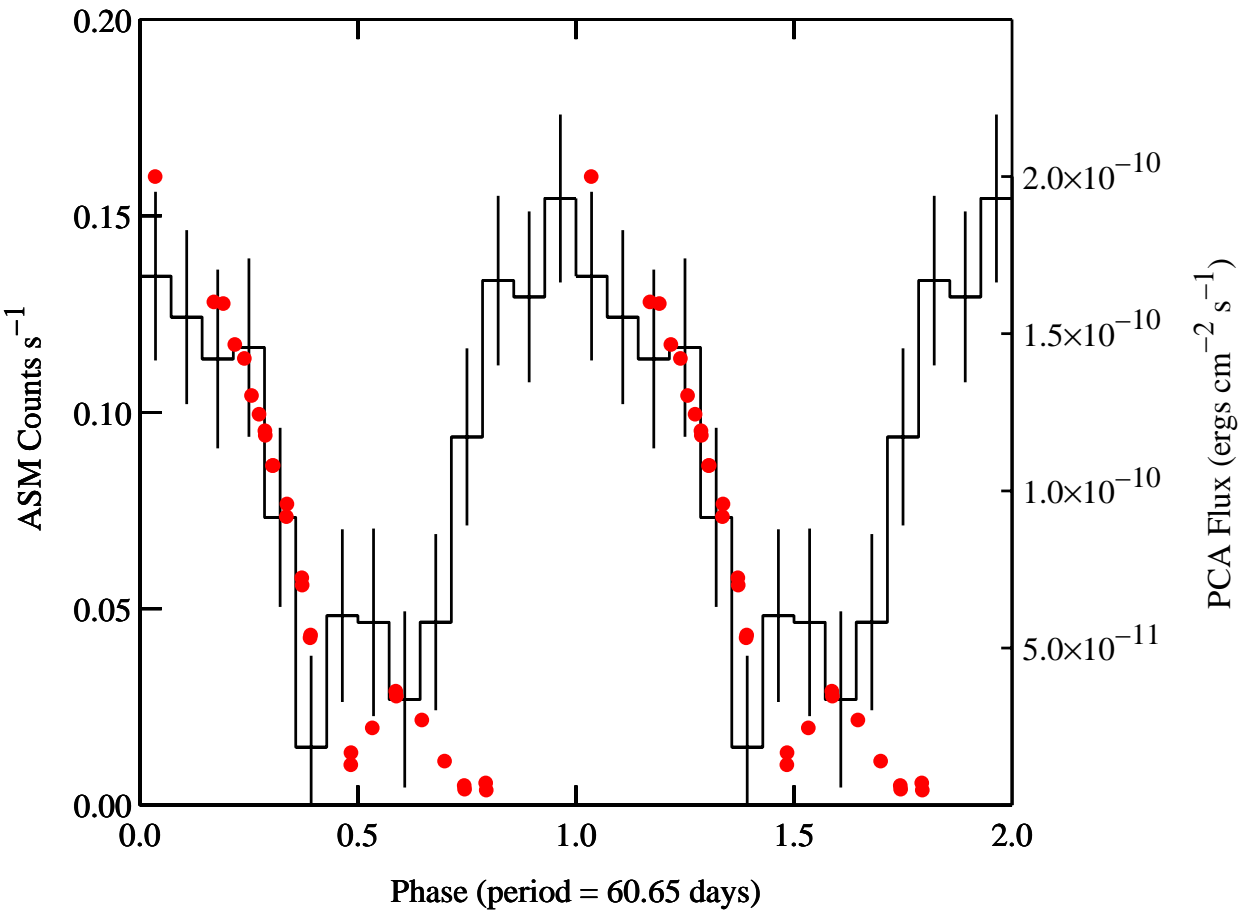


Fig. 4.— *RXTE* ASM light curve of XTTE J1859+083 since MJD 50,460 folded on the proposed orbital period (histogram with error bars). The dots show the PCA fluxes scaled to the ASM light curve to facilitate a comparison of the morphology of the folded ASM light curve with the PCA light curve. Note that the fluxes measured with the PCA are much higher than the mean ASM flux ($0.1 \text{ ASM counts s}^{-1} \simeq 3.1 \times 10^{-11} \text{ ergs s}^{-1}$) because the ASM folded light curve also includes low flux states.. Phase zero corresponds to MJD 52,549.1.

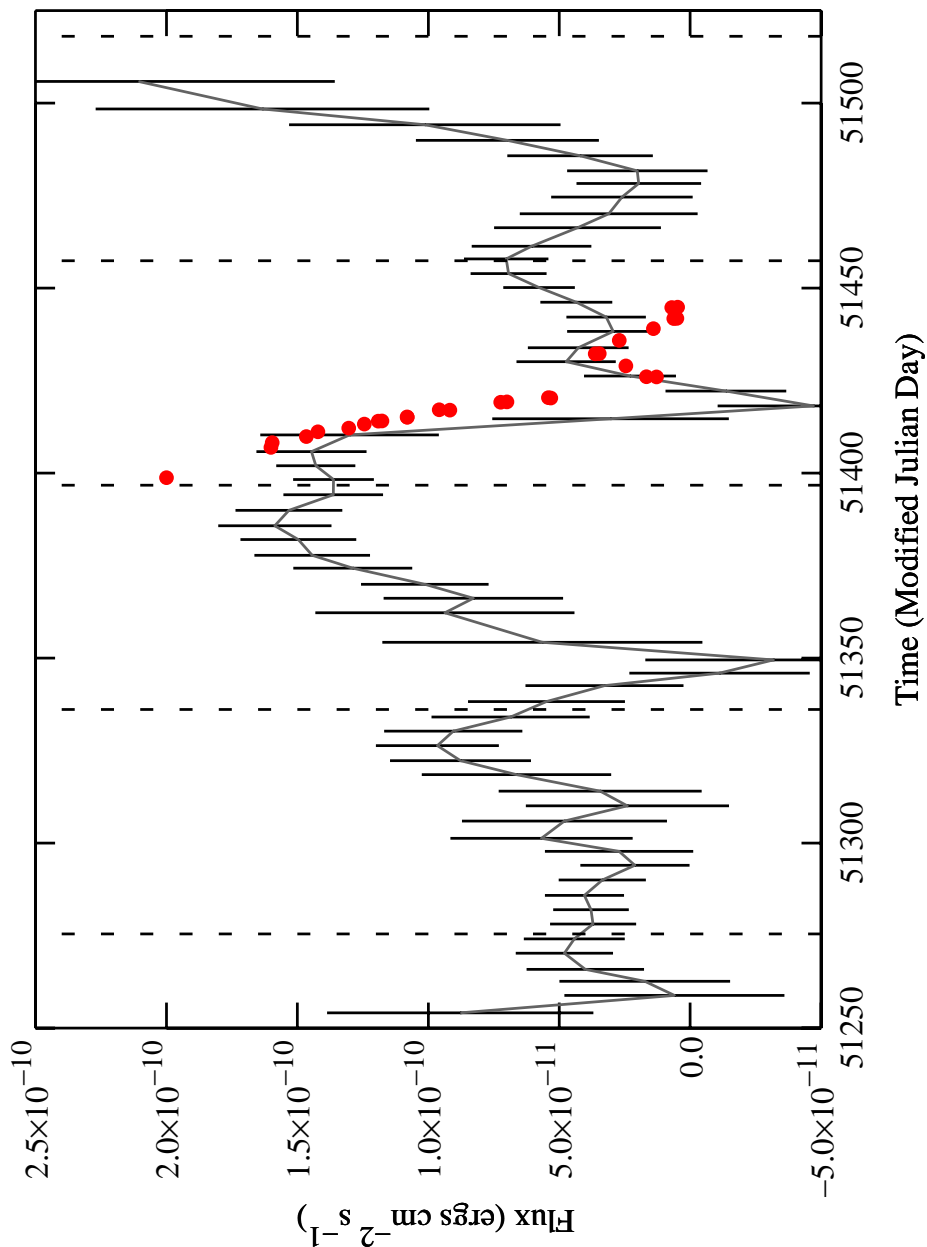


Fig. 5.— ASM light curve of XTE J1859+083 (lines with error bars) around the time when the PCA observations were made. The time resolution is 5 days and the light curve has been smoothed using the algorithm described in Section 2.2. The red dots show the PCA fluxes. The vertical dashed lines indicate the times of predicted maximum flux based on the possible 60.65 day period.

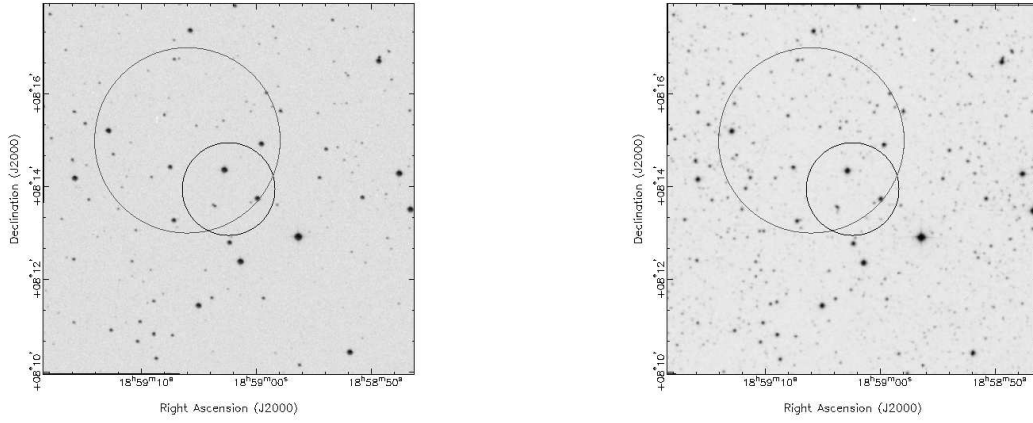


Fig. 6.— Error circles for the position of XTE J1859+083 on Digitized Sky Survey images covering the DSS blue (left) and red (right) bands. North is up and East to the left. The larger error circle to the North East is the *RXTE* PCA error region from Marshall et al. (1999) and the smaller circle is from the *BeppoSAX* WFC observations presented here.